Two-photon-state generation via four-wave mixing in optical fibers

Jun Chen, Xiaoying Li, and Prem Kumar
Center for Photonic Communication and Computing, ECE Department, Northwestern University, Evanston, Illinois 60208-3118, USA
(Received 20 March 2005; published 2 September 2005)

A quantum theory of two-photon-state generation via four-wave mixing in optical fibers is studied, with emphasis on the case where the pump is a classical, narrow (picosecond-duration) pulse. One of the experiments performed in our lab is discussed and analyzed. Numerical predictions from the theory are shown to be in good agreement with the experimental results.

DOI: 10.1103/PhysRevA.72.033801 PACS number(s): 42.65.Lm, 42.50.Dv

I. INTRODUCTION

Four-wave mixing (FWM) has long been studied, especially in the context of isotropic materials, e.g., optical fibers [1,2]. Generally speaking, it is a photon-photon scattering process, during which two photons from a relatively high-intensity beam, called pump, scatter through the third-order nonlinearity ($\chi^{(3)}$) of the material (silica glass in the case of optical fibers) to generate two daughter photons, called signal and idler photons, respectively. The frequencies of the daughter photons are symmetrically displaced from the pump frequency, satisfying the energy conservation relation: $\omega_s + \omega_i = 2\omega_p$, where ω_j $(j=p,s,i)$ denotes the pump/signal/idler frequency, respectively. They are predominantly copolarized with the pump beam, owing to the isotropic nature of the optical Kerr nonlinearity: $\chi^{(3)}_{xxxx} = \chi^{(3)}_{xxyy} + \chi^{(3)}_{xyxy} + \chi^{(3)}_{xyyx} = 3\chi^{(3)}_{xxyy}$. The daughter photons also form a time-energy-entangled state, in the sense that the two-particle wave function cannot be factorized into products of single-particle wave functions: $\Psi(\omega_s, \omega_i) \neq \zeta(\omega_s) \cdot \varphi(\omega_i)$. This four-photon scattering process is intrinsically interesting and particularly useful when applied to the field of quantum information processing (QIP), in which generation of entangled states and test of Bell's inequalities play an important role.

A great amount of original work, both theoretical and experimental, has been done in the rapidly expanding field of QIP (see for example [3] for a general review). The workhorse process for generating entangled states is the process of spontaneous parametric down conversion (SPDC) in second-order ($\chi^{(2)}$) nonlinear crystals, which has been studied exhaustively during the past decades. However, unlike its $\chi^{(2)}$ counterpart, the $\chi^{(3)}$ process of FWM has received relatively lesser theoretical attention in the quantum-mechanical framework, despite its apparent benefits in the applications of quantum information processing. To name a few, the ubiquitous readily available fiber plant serves as a perfect transmission channel for the FWM-generated entangled qubits, whereas it remains a technical challenge to efficiently couple $\chi^{(2)}$-generated entangled photons into optical fibers due to mode mismatch. Besides, the excellent single-mode purity of the former makes it suitable for applications which require multiple quantum interactions. Furthermore, it is also possible to wavelength multiplex several different entangled channels from the broadband parametric spectrum of FWM by utilizing the advanced multiplexing/demultimplexing devices developed in connection with the modern fiber-optic communications infrastructure. The only drawback of this scheme that has been identified is the process of spontaneous Raman scattering (SRS), which inevitably occurs in any $\chi^{(3)}$ medium and generates uncorrelated photons into the detection bands, leading to a degradation in the quality of the generated entanglement [4]. Various efforts have been made to minimize the negative effect that SRS imposes [5].

In this paper, we present a quantum theory that models the FWM process in an optical fiber, without inclusion of the Raman effect. The pump is treated as a classical narrow (picosecond-duration) pulse due to its experimental relevance. The signal and idler fields form a quantum mechanical two-photon (or "biphoton" [6,7]) state at the output of the fiber. From the experimental point of view, what we are mostly interested in is the non-classicality that the two-photon state exhibits. It is this unique quantum feature that makes the two-photon state a valid candidate for various quantum-entanglement related experiments, including quantum cryptography [8], quantum teleportation [9], etc. Coincidence-photon counting, or second-order coherence measurement of the optical field [10], serves as a measurement technique that distinguishes a quantum-mechanically-entangled state from a classically-correlated state, which will form a central part of our investigation. The paper is organized as follows. We first set up the theoretical problem by briefly describing the experimental setup and the photon-counting results in Sec. II. Section III begins with a brief review of the coupled-wave equations from the classical FWM theory. We then derive the quantum equations of motion from their classical counterparts in accordance with the correspondence principle. The interaction Hamiltonian which leads to these quantum equations of motion is determined, and subsequently employed in calculating the $\chi^{(3)}$ two-photon state. A comparison chart between the $\chi^{(3)}$ and $\chi^{(2)}$ biphotons summarizes this section. In Secs. IV and V, single-photon and coincidence-photon counting formulas for the $\chi^{(3)}$ two-photon state are derived. Section VI compares the experimental results with the theoretical predictions. Finally, conclusions are drawn in Sec. VII.

II. BRIEF DESCRIPTION OF THE EXPERIMENT

In this section we briefly review our experiments from Ref. [11], whose results will later be compared with the

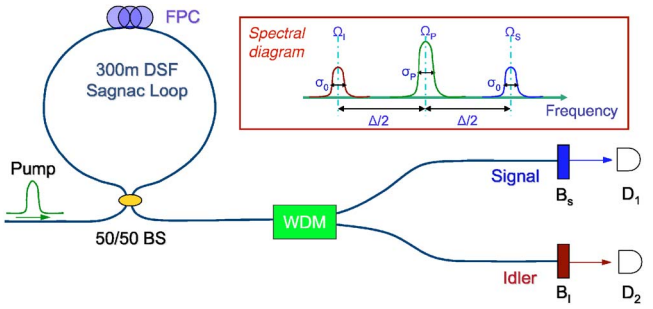

FIG. 1. (Color online) A schematic of the experimental setup. FPC, fiber polarization controller; BS, beam splitter; B_s, B_i, Gaussian filters; D_1, D_2, photon-counting detectors. Inset shows the spectral diagram of the pump, signal, and idler fields. Ω_p, pump central frequency; Ω_s, signal central frequency; Ω_i, idler central frequency; σ_p, pump bandwidth (FWHM); σ_0, filter bandwidth (FWHM); $\Delta/2$, central frequency difference between the pump and idler (or the signal and pump).

theory. Consider the schematic experimental setup shown in Fig. 1. The pump consists of a train of narrow pulses (~5 ps duration) from a Ti-sapphire-laser pumped optical-parametric oscillator (OPO). It is launched into a Sagnac loop of dispersion-shifted fiber (DSF), in which FWM occurs when the phase-matching condition is satisfied. Most of the pump photons are reflected back due to the mirrorlike property of the Sagnac loop [13]. A dual-band spectral filter is employed at the output of the Sagnac loop to further separate the signal part of the two-photon state from the idler part. The dual-band spectral filter can be effectively modelled by a wavelength-division (de)multiplexer (WDM) plus a pair of Gaussian-shaped bandpass filters. After filtering, the two spatially separated streams of photons are directed to a pair of avalanche photodiodes (APD) capable of single-photon detection and photon counting. Results, including the single-photon counting rate and the coincidence-photon counting rate, are recorded during the experiment and stored in a computer for later data retrieval and processing. The inset graph ("*Spectral Diagram*") in Fig. 1 defines the various system parameters by their corresponding mathematical symbols, which will be used throughout our theory framework.

A sample coincidence-counting result from Ref. [11] is shown in Fig. 2. The top (bottom) series of data points represents the total (accidental) coincidence-count rate as a function of the single-channel count rate. SRS and dark counts from the detectors account for the major part of the accidental coincidence counts. Our to-be-developed theory, however, only takes into account the photon counts generated by the FWM process. In order to reconcile the theory with experiments, the contributions from SRS and dark counts from the detectors are independently measured [5], and subsequently subtracted from both the single counts and the total coincidence counts. Overall quantum efficiencies of detection in both the signal and idler channels are also separately measured. The single-count rates are divided by the respective quantum efficiencies and the coincidence-count rate by the product of the efficiencies in the signal and idler channels to arrive at rates at the output of the fiber for comparison with the prediction of our theory. The dependence of

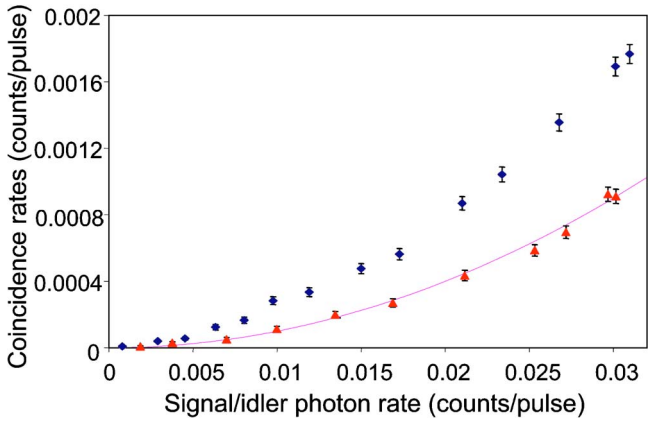

FIG. 2. (Color online) Experimental results. Diamonds, total coincidences; triangles, accidental coincidences; curve, theoretical fit $y=x^2$ for statistically independent photon sources.

the photon-counting results on various system parameters, for instance the pump power, pump bandwidth, and filter bandwidth, etc., can be studied.

Polarization entanglement has also been generated by time and polarization multiplexing two such FWM processes [12]. However, the theory for that particular experiment is a straightforward extension of our current theory, and therefore will not be included in the analysis to follow.

III. THE INTERACTION HAMILTONIAN AND THE TWO-PHOTON STATE

Having described the experiment in the previous section, we are ready to start building up the theoretical model for that experiment. We take the standard approach of modern quantum optics, i.e., finding out the interaction Hamiltonian and calculating the evolution of the state vector using the Schrödinger picture. We accomplish the first task by seeking connections with the well-known classical FWM theory in optical fibers [2]. The coupled classical-wave equations for the pump, signal, and idler fields are

$$\frac{\partial A_p}{\partial z} = i\gamma|A_p|^2 A_p,$$

$$\frac{\partial A_s}{\partial z} = i\gamma[2|A_p|^2 A_s + A_p^2 A_i^* e^{-i\Delta kz}],$$

$$\frac{\partial A_i}{\partial z} = i\gamma[2|A_p|^2 A_i + A_p^2 A_s^* e^{-i\Delta kz}], \quad (1)$$

where the usual undepleted-pump approximation has been made, and we only keep terms that are significant, i.e., to $O(A_p^2)$. Fiber loss is neglected from the above equations. The A_j $(j=p,s,i)$ denote electric-field amplitudes for the pump, signal, and idler, respectively, and all of them have been normalized such that their unit is $\sqrt{\mathrm{W}}$. $\Delta k=k_s+k_i-2k_p$ is the magnitude of the wave-vector mismatch. $\gamma=2\pi n_2/\lambda A_{\mathrm{eff}}$ is the nonlinear parameter of interaction, wherein $n_2=(3/4n^2\epsilon_0 c)\mathrm{Re}(\chi^{(3)}_{xxxx})$ is the nonlinear-index coefficient, ϵ_0 is

the vacuum permittivity, A_{eff} is the effective mode area of the optical fiber, and $\lambda \approx \lambda_{p,s,i}$ is the wavelength involved in the FWM interaction.

Due to the highly nonresonant nature of FWM in optical fibers, we expect the quantum equations of motion, which describe the interplay between and evolution of the fields at the photon level, to fully correspond with their classical counterparts. In light of this correspondence principle, we write the quantum equations of motion by simply replacing the classical amplitudes in Eqs. (1) with electric-field operators:

$$\frac{\partial E_p^{(+)}}{\partial z} = i\eta E_p^{(-)} E_p^{(+)} E_p^{(+)},$$

$$\frac{\partial E_s^{(+)}}{\partial z} = i\eta [2E_p^{(-)} E_p^{(+)} E_s^{(+)} + E_i^{(-)} E_p^{(+)} E_p^{(+)}],$$

$$\frac{\partial E_i^{(+)}}{\partial z} = i\eta [2E_p^{(-)} E_p^{(+)} E_i^{(+)} + E_s^{(-)} E_p^{(+)} E_p^{(+)}], \tag{2}$$

where $E_j^{(+)} = \sqrt{(\hbar\omega_j / 2\epsilon_0 V_Q)} a_j$ $(j = p, s, i)$ are the positive-frequency electric-field operators, corresponding to photon annihilation operators, and V_Q is the quantization volume. Here we omit the Hermitian-conjugate equations corresponding to Eqs. (2) for simplicity. We have assumed that the photon fields phase match, i.e., $\Delta k = 0$. In Eqs. (2), $\eta = -\chi^{(3)} A_{\text{eff}} nL\omega / 2V_Q c$ is a constant similar to γ in the classical equations (1); the exact form of this constant differs from its classical cousin to compensate for the unit discrepancy between the two sets of equations (note that the operator $E_j^{(+)}$ is of unit V/m, and the amplitude A_j is of unit $\sqrt{\text{W}}$). The correct form of the interaction Hamiltonian that we are seeking should lead to Eqs. (2) via the Heisenberg equation of motion for the field operators, namely, $i\hbar(\partial \hat{E} / \partial t) = [\hat{E}, H_I]$, where $\hat{E}$ stands for any electric-field operator. Utilizing the mathematical facts $\partial / \partial t \equiv (c/n)(\partial / \partial z)$ and $[E_j^{(+)}(z), E_k^{(-)}(z')] = (\hbar\omega / 2\epsilon_0 V_Q)\delta(z - z')\delta_{jk}$, we arrive at the following form for our interaction Hamiltonian:

$$\begin{aligned} H_I = \beta\epsilon_0 \chi^{(3)} \int_V dV [& E_p^{(-)} E_p^{(-)} E_p^{(+)} E_p^{(+)} + 2E_s^{(-)} E_i^{(-)} E_p^{(+)} E_p^{(+)} \\ & + 2E_p^{(-)} E_p^{(-)} E_s^{(+)} E_i^{(+)} + 4E_p^{(-)} E_p^{(+)} E_s^{(-)} E_s^{(+)} \\ & + 4E_p^{(-)} E_p^{(+)} E_i^{(-)} E_i^{(+)}], \end{aligned} \tag{3}$$

where β is an overall unknown constant related to the specific experimental details, which will be determined later when we compare our theory with the experiment; $\chi^{(3)}$ is the nonlinear electric susceptibility whose tensorial nature is ignored since all the optical fields are assumed to be linearly copolarized. The integral is taken over the entire volume of interaction, namely, the effective volume of the optical fiber. We label the first term in the integrand of Eq. (3) as the self-phase modulation (SPM) of the pump field, the next two terms as the four-photon scattering (FPS) among the optical fields, and the last two terms as the cross-phase modulation (XPM) between pump and signal (idler)fields.

After obtaining the Hamiltonian responsible for the quantum FWM process, we are ready to tackle our next task: calculate the state vector evolution. It is worthwhile, at this point, to define the various electric field operators appearing in the Hamiltonian, in accordance with the experiment we are trying to model. The pump field is taken to be a classical narrow pulse, which is linearly polarized, propagating in the z direction (parallel with the fiber axis), with a central frequency Ω_p and an envelope of arbitrary shape $\tilde{E}_p$. Mathematically, it can be written as

$$E_p^{(+)} = e^{-i\Omega_p t} \widetilde{E_p}(z,t) = e^{-i\Omega_p t} \int d\nu_p \bar{E}_p(\nu_p) e^{ik_p z - i\nu_p t}, \tag{4}$$

wherein the bandwidth of the pump field is much smaller than Ω_p, satisfying the quasi-monochromatic approximation. The signal and idler fields are quantized electromagnetic fields, copolarized and copropagating with the pump, as given by the following multimode expansion:

$$E_s^{(-)} = \sum_{\omega_s} \sqrt{\frac{\hbar\omega_s}{2\epsilon_0 V_Q}} \frac{a_{k_s}^\dagger}{n(\omega_s)} e^{-i[k_s(\omega_s)z - \omega_s t]}, \tag{5}$$

$$E_i^{(-)} = \sum_{\omega_i} \sqrt{\frac{\hbar\omega_i}{2\epsilon_0 V_Q}} \frac{a_{k_i}^\dagger}{n(\omega_i)} e^{-i[k_i(\omega_i)z - \omega_i t]}, \tag{6}$$

where $a_{k_s}^\dagger$ is the creation operator for the signal mode with frequency ω_s, $k_s(\omega_s) = n(\omega_s)\omega_s / c$ is its wave-vector magnitude. The idler field is defined in an analogous fashion. The central frequencies of the signal and idler fields are individually denoted by Ω_s and Ω_i, which are symmetrically distanced from the central frequency of the pump field Ω_p, satisfying the energy conservation relation: $\Omega_s + \Omega_i = 2\Omega_p$.

To simplify our calculation and to compare our results with the experiments, two assumptions are further made about the pump field: it has a Gaussian spectral envelope and its SPM is included in a straightforward manner, i.e.,

$$E_p^{(+)} = e^{-i\Omega_p t} e^{-i\gamma P_p z} E_{p0} \int d\nu_p e^{-\nu_p^2 / 2\sigma_p^2} e^{ik_p z - i\nu_p t}, \tag{7}$$

where $P_p \equiv 2\sqrt{\pi} A_{\text{eff}} \epsilon_0 cn\sigma_p^2 E_{p0}^2$ is the peak power of the pump pulse, which is treated as a constant under the undepleted pump approximation, and σ_p is the optical bandwidth of the pump. The first assumption is justified by the fact that our experimental optical filter for the pump can be well approximated by a Gaussian function in the frequency domain. The validity of the second assumption can be seen when we solve the classical equation of motion for the pump field, namely, the complex conjugate form of the first equation in Eqs. (1), which reads

$$\frac{\partial A_p^*}{\partial z} = -i\gamma |A_p|^2 A_p^*. \tag{8}$$

We choose to study the complex conjugate form of the equation because it is A_p^* that corresponds to $E_p^{(+)}$. Straightforward calculations show that the solution to Eq. (8) is $A_p^*(z) = A_p^*(0) e^{-i\gamma P_p z}$, where $P_p = |A_p|^2$ is the same undepleted peak power of the pump pulse. The SPM term of the pump,

$e^{-i\gamma P_p z}$, which is the nonlinear phase factor in the classical FWM theory that determines the phase-matching condition [2], now manifests itself in our quantum-mechanical calculation as a "phase tag" for the pump field through its propagation along the optical fiber. Finally, the undepleted-pump approximation holds because the loss in the fiber is negligible and only a few photons are scattered ($\sim$1 out of 10^8) through the nonlinear interaction.

The two-photon state at the output of the fiber is calculated by means of first-order perturbation theory, i.e.,

$$|\Psi\rangle = |0\rangle + \frac{1}{i\hbar}\int_{-\infty}^{\infty} H_I(t)dt|0\rangle. \tag{9}$$

Retaining of higher-order terms in the perturbation series involves generation of multi-photon states, which will be ignored in our calculation owing to their smallness. We can see that only the FPS terms in the interaction Hamiltonian contribute to the formation of the signal/idler two-photon state. This is because all terms vanish when acting on the vacuum state $|0\rangle$ with the exception of $E_s^{(-)}E_i^{(-)}E_p^{(+)}E_p^{(+)}$+H.c., which we denote as

$$H_{\mathrm{FPS}} \equiv \alpha\epsilon_0\chi^{(3)}\int_V dV(E_s^{(-)}E_i^{(-)}E_p^{(+)}E_p^{(+)} + \mathrm{H.c.}), \tag{10}$$

where $\alpha=2\beta$, and H.c. stands for Hermitian conjugate.

The state vector is then given by

$$|\Psi\rangle = |0\rangle + \frac{1}{i\hbar}\int_{-\infty}^{\infty} H_{\mathrm{FPS}}dt|0\rangle, \tag{11}$$

which is a superposition of the vacuum and the two-photon state. Equations (5)–(7) and (10), when put into Eq. (11), after some algebra, lead to the following form of the state vector:

$$|\Psi\rangle = |0\rangle + \sum_{k_s,k_i} F(k_s,k_i)a_{k_s}^{\dagger}a_{k_i}^{\dagger}|0\rangle, \tag{12}$$

$$F(k_s,k_i) = g\int_{-L}^{0} dz \frac{1}{\sqrt{1-ik''(\Omega_p)\sigma_p^2 z}} \exp\left\{-\frac{ik''(\Omega_p)z}{4}(\nu_s-\nu_i+\Delta)^2 - 2i\gamma P_p z - \frac{(\nu_s+\nu_i)^2}{4\sigma_p^2}\right\}, \tag{13}$$

$$g = \frac{\alpha\pi^2\chi^{(3)}P_p}{i\epsilon_0 V_Q n^3 \lambda_p \sigma_p}. \tag{14}$$

The function $F(k_s,k_i)$ is called the two-photon spectral function [7]. Here $k''(\Omega_p)=(d^2k/d\omega^2)|_{\omega=\Omega_p}$ is the second-order dispersion at the pump central frequency (also known as the group-velocity dispersion, or GVD for short), which can be obtained from $k''(\Omega_p)=-(\lambda_p^2/2\pi c)D_{\mathrm{slope}}(\lambda_p-\lambda_0)$, where λ_0 is the zero-dispersion wavelength of the DSF, $D_{\mathrm{slope}}=0.06$ ps/(nm$^2\cdot$km) is the experimental value of the dispersion slope in the vicinity of λ_0. $\Delta\equiv\Omega_s-\Omega_i$ is the central-frequency difference between signal and idler fields. The ν_s and ν_i are related to ω_s and ω_i through the following relation: $\nu_s=\omega_s-\Omega_s$, $\nu_i=\omega_i-\Omega_i$.

In lieu of giving the detailed derivation of the two-photon state (which is lengthy), we highlight several noteworthy mathematical maneuvers along the way. The following identification of the Dirac δ-function is useful in handling the time integral,

$$\int_{-\infty}^{\infty} e^{i(\omega+\omega'-2\Omega_p-\nu_p-\nu_p')t}dt = 2\pi\delta(\omega+\omega'-2\Omega_p-\nu_p-\nu_p'), \tag{15}$$

which reinforces the energy conservation requirement in the four-photon scattering process. The volume integral $\int dV$ is reduced to a length integral $\int dz$ by using $\int\int dxdy \rightarrow A_{\mathrm{eff}}$, which is a valid approximation for single spatial-mode propagation and interaction in optical fibers. Taylor expansion of the various wave-vector magnitudes k_p, k_s, k_i around the pump central frequency Ω_p has been used to simplify their relationship. In terms of the mathematical structure of the two-photon spectral function, we note that the GVD term $k''(\Omega_p)$ as well as the pump SPM term $\gamma P_p z$ play important roles in shaping the two-photon state, in contrast with the observation that the pump SPM term is virtually nonexistent in the $\chi^{(2)}$-generated two-photon states. The appearance of the pump SPM is therefore a unique signature of the $\chi^{(3)}$ two-photon state, when comparing with its $\chi^{(2)}$ counterparts. To outline the differences and similarities among the various two-photon states, a comparison chart is provided in Fig. 3.

IV. SINGLE-PHOTON COUNTING RATE

In this and the next section, we will make use of the previously derived formulas for the two-photon state [Eqs. (12)–(14)] to obtain the photon-counting formulas for the single channels as well as for the coincidences. The mathematics involved for the two cases are similar to each other, so it suffices to present a detailed version for the former. The signal-band single-photon counting rate can be calculated using the following formula [10]:

	$\chi^{(3)}$	$\chi^{(2)}$ Type-I	$\chi^{(2)}$ Type-II
Frequency	Non-degenerate	Degenerate / Non-degenerate	Degenerate / Non-degenerate
Spatial direction	Collinear	Collinear / Non-collinear	Collinear / Non-collinear
Polarization	↑↑↑	⊙⊙ ↑	⊙ ↑ ↑
SPM	✓		
First-order dispersion			✓
GVD	✓	✓	

FIG. 3. (Color online) A comparison chart of the various $\chi^{(2)}$ and $\chi^{(3)}$ biphotons. The check mark denotes that the effect is critically important.

$$S_c = \int_0^\infty \langle \Psi | E_s^{(-)} E_s^{(+)} | \Psi \rangle dT. \tag{16}$$

It is obvious that an analogous approach can be applied to the idler band as well.

As S_c denotes single-photon counting probability for one pump pulse, it is by definition a dimensionless quantity. It is customary, in this case, to use the photon-number unit for the electric field operator [14]. In this unit, the electric field operator has dimensionality $1/\sqrt{\text{sec}}$, as shown below:

$$E_s^{(+)} = \sum_{k_s} \sqrt{\frac{cA_{\text{eff}}}{4V_Q}} a_{k_s} e^{-i\omega_s t} e^{-(\omega_s - \Omega_s)^2/2\sigma_0^2}, \tag{17}$$

where the Gaussian filter in front of the detector has been included. The integrand in Eq. (16) can be written as

$$\langle \Psi | E_s^{(-)} E_s^{(+)} | \Psi \rangle = \frac{cA_{\text{eff}}}{4V_Q} \sum_{k_i, k_i'} \langle 0 | a_{k_i} a_{k_i'}^\dagger | 0 \rangle \sum_{k_1, k_2, k_s, k_s'} \langle 0 | a_{k_s} a_{k_1}^\dagger a_{k_2} a_{k_s'}^\dagger | 0 \rangle e^{i\omega_s t} e^{-(\omega_s - \Omega_s)^2/2\sigma_0^2} e^{-i\omega_s' t} e^{-(\omega_s' - \Omega_s)^2/2\sigma_0^2} F^*(k_s, k_i) F(k_s', k_i'). \tag{18}$$

Nonvanishing results emerge only when the wave vectors observe the following restrictions:

$$k_i = k_i', \quad k_s = k_1, \quad k_s' = k_2. \tag{19}$$

The integrand may be further simplified into

$$\begin{aligned} \langle \Psi | E_s^{(-)} E_s^{(+)} | \Psi \rangle &= \frac{cA_{\text{eff}}}{4V_Q} \sum_{k_i} \left(\sum_{k_s} e^{i\omega_s t} e^{-(\omega_s - \Omega_s)^2/2\sigma_0^2} F^*(k_s, k_i) \right) \cdot \left(\sum_{k_s'} e^{-i\omega_s' t} e^{-(\omega_s' - \Omega_s)^2/2\sigma_0^2} F(k_s', k_i) \right) \\ &= \frac{cA_{\text{eff}}}{32\pi^3 u(\omega_i) u^2(\omega_s)} \int d\omega_i \left| \int d\omega_s e^{-i\omega_s t} e^{-(\omega_s - \Omega_s)^2/2\sigma_0^2} F(\omega_s, \omega_i) \right|^2, \end{aligned} \tag{20}$$

where in the last step we have invoked the following identity to transform wave-vector summations into angular frequency integrals:

$$\sum_{k_j} \to \frac{V_Q^{1/3}}{2\pi} \int dk_j = \frac{V_Q^{1/3}}{2\pi} \int \frac{d\omega_j}{u(\omega_j)}. \tag{21}$$

Here $u(\omega_j) = d\omega_j / dk_j, j = s, i$ is the group velocity of the j mode, and is to be taken as a constant c/n in our simplified calculation.

Equation (16) can be written in the following form after all the above steps have been absorbed:

$$\begin{aligned} S_c = &\frac{\pi^2 \alpha^2 [\chi^{(3)}]^2 A_{\text{eff}} P_p^2}{16\epsilon_0^2 V_Q^2 n^3 c^2 \lambda_p^2 \sigma_p^2} \int_{-L}^0 dz_1 \int_{-L}^0 dz_2 \frac{e^{-2i\gamma P_p (z_1 - z_2)}}{\sqrt{(1 - ik'' \sigma_p^2 z_1)(1 + ik'' \sigma_p^2 z_2)}} \int d\nu_s \int d\nu_i \\ &\times \exp\left\{ -\frac{(\nu_s + \nu_i)^2}{2\sigma_p^2} - \frac{\nu_s^2}{\sigma_0^2} - i\frac{k''}{4} (z_1 - z_2)(\nu_s - \nu_i + \Delta)^2 \right\}. \end{aligned} \tag{22}$$

The frequency double integral can be analytically integrated through a change of variables and completion of squares, namely, let

$$\nu_+ = \frac{\nu_s + \nu_i}{2}, \tag{23}$$

$$\nu_- = \nu_s - \nu_i. \tag{24}$$

The frequency double integral can be rewritten in terms of the new variables as

$$\int d\nu_s \int d\nu_i e^{-(\nu_s+\nu_i)^2/2\sigma_p^2 - \nu_s^2/\sigma_0^2 - i(k''/4)(z_1-z_2)(\nu_s-\nu_i+\Delta)^2}$$
$$= \int d\nu_+ \exp\left\{-\frac{2\sigma_0^2+\sigma_p^2}{\sigma_0^2\sigma_p^2}\left[\nu_+ + \frac{\sigma_p^2\nu_-}{2(2\sigma_0^2+\sigma_p^2)}\right]^2\right\}$$
$$\times \int d\nu_- \exp\left\{-\frac{\nu_-^2}{2(2\sigma_0^2+\sigma_p^2)} - \frac{ik''(z_1-z_2)(\nu_-+\Delta)^2}{4}\right\}. \tag{25}$$

The first part of the integral, concerning only Gaussian functions with real variable as arguments, is easily integrated as

$$\int d\nu_+ \exp\left\{-\frac{2\sigma_0^2+\sigma_p^2}{\sigma_0^2\sigma_p^2}\left[\nu_+ + \frac{\sigma_p^2\nu_-}{2(2\sigma_0^2+\sigma_p^2)}\right]^2\right\}$$
$$= \frac{\sqrt{\pi}\sigma_p\sigma_0}{\sqrt{2\sigma_0^2+\sigma_p^2}}. \tag{26}$$

The second part of the integral, having a Gaussian function with complex argument as integrand, has a closed analytical form by using the integral formula from Ref. [15], i.e.,

$$\int d\nu_- \exp\left\{-\frac{\nu_-^2}{2(2\sigma_0^2+\sigma_p^2)} - \frac{ik''(z_1-z_2)(\nu_-+\Delta)^2}{4}\right\}$$
$$= \frac{\sqrt{\pi}}{\sqrt{a}\sqrt[4]{1+b^2}} \exp\left[-\frac{cb^2}{1+b^2} + \frac{i}{2}\arctan(b) + \frac{ir}{1+b^2}\right], \tag{27}$$

where $a=1/2(2\sigma_0^2+\sigma_p^2)$, $b=-k''(z_1-z_2)(2\sigma_0^2+\sigma_p^2)/2$, $c=\Delta^2/2(2\sigma_0^2+\sigma_p^2)$, and $r=-k''(z_1-z_2)\Delta^2/4$.

We therefore obtain the following final form of the single-photon counting formula:

$$S_c = A_1(\gamma P_p L)^2 \frac{\sigma_0}{\sigma_p} I_{\mathrm{sc}}, \tag{28}$$

$$A_1 = \frac{\alpha^2 \pi n A_{\mathrm{eff}}^3}{18\sqrt{2}V_Q^2}, \tag{29}$$

$$I_{\mathrm{sc}} = \frac{1}{L^2}\int_{-L}^{0} dz_1 \int_{-L}^{0} dz_2 \frac{\exp\left[-2i\gamma P_p(z_1-z_2) - \frac{cb^2}{1+b^2} + \frac{i}{2}\arctan(b) + \frac{ir}{1+b^2}\right]}{\sqrt{(1-ik''\sigma_p^2 z_1)(1+ik''\sigma_p^2 z_2)}\sqrt[4]{1+b^2}}, \tag{30}$$

where A_1 is an unknown constant with α and V_Q as fitting parameters, I_{sc} is a double-length integral which has to be investigated numerically. Despite the seemingly complicated form of the single-counts formula, the physics behind it is quite clear. Apart from a small contribution from the double integral, the single counts scale quadratically with pump power, which coincides with the intuitive four-photon scattering picture that requires 2 pump photons to scatter into the signal/idler modes. It also scales linearly with the ratio of the filter bandwidth to pump bandwidth. This makes sense in that if one broadens the filter bandwidth, more photons will be collected; and conversely if the filter bandwidth is narrowed, one would expect to count less photons. The dependence on pump bandwidth is more clearly seen in the time domain. As the pulse width becomes wider (thus the pump bandwidth narrower) while maintaining the peak power to be the same, the probability of four-photon scattering increases linearly with pulse width (thus decreases linearly with pump bandwidth) simply because there is more time for the pump photons to interact; the reverse is also true. The more intricate dependence on pump power, pump bandwidth and filter bandwidth is described by the double integral I_{sc}, which takes into account phase matching, SPM of the pump, and the Gaussian shapes of pump and filter spectrum.

V. COINCIDENCE-PHOTON COUNTING RATE

Calculations of the coincidence-counting rate with Gaussian filters can be performed in a similar way to those of the single counting rate. We start with the probability of getting a coincidence count for each pulse [10]:

$$C_c = \int_0^\infty dT_1 \int_0^\infty dT_2 \langle\Psi|E_1^{(-)}E_2^{(-)}E_2^{(+)}E_1^{(+)}|\Psi\rangle. \tag{31}$$

The electric fields are free fields propagating through Gaussian filters evaluated at detectors 1 and 2, defined in the photon-number unit:

$$E_1^{(+)} = \sum_{k_1} \sqrt{\frac{cA_{\mathrm{eff}}}{4V_Q}} a_{k_1} e^{-i\omega_s t_1} e^{-(\omega_s-\Omega_s)^2/2\sigma_0^2}, \tag{32}$$

$$E_2^{(+)} = \sum_{k_2} \sqrt{\frac{cA_{\text{eff}}}{4V_Q}} a_{k_2} e^{-i\omega_i t_2} e^{-(\omega_i - \Omega_i)^2/2\sigma_0^2}, \tag{33}$$

where the Gaussian filters take the form $f(\omega_j - \Omega_j) = f_j e^{-(\omega_j - \Omega_j)^2/2\sigma_j^2}$, $f_j = 1$, and $\sigma_j = \sigma_0$ for $j = s, i$ are assumed to simplify the calculation. $t_i = T_i - l_i/c$ is the time at which the biphoton wave packet leaves the output tip of the fiber, which in our case is almost the same for the signal and idler as there is negligible group-velocity difference between the two closely spaced (in wavelength), copolarized fields. l_i denotes the optical path length from the output tip of the fiber to the detector i, $i = 1, 2$, and can be carefully path matched to be the same.

The integrand in Eq. (31) can be written in the following form:

$$\langle \Psi | E_1^{(-)} E_2^{(-)} E_2^{(+)} E_1^{(+)} | \Psi \rangle = |\langle 0 | E_2^{(+)} E_1^{(+)} | \Psi \rangle|^2 = |A(t_1, t_2)|^2, \tag{34}$$

where $A(t_1, t_2)$ is the *biphoton amplitude* introduced in Refs. [6,7]. While the concept of a biphoton amplitude plays an important role in the study of frequency and wave-number entanglement inherent in the two-photon state, it serves merely as a calculational shorthand for our purpose in determining the coincidence counting rate. It is straightforward to show that

$$A(t_1, t_2) = \frac{cA_{\text{eff}}}{4V_Q} \sum_{k_s, k_i} F(k_s, k_i) e^{-i(\omega_s t_1 + \omega_i t_2)} e^{-(\nu_s^2 + \nu_i^2)/2\sigma_0^2}. \tag{35}$$

The fact that the biphoton cannot be written as a function of t_1 times a function of t_2 may be readily observed from the form that Eq. (35) takes. It is also nonfactorable in the wave numbers k_s and k_i, displaying its entangled nature in those degrees of freedom. However it's not entangled in polarization, due to the fact that all the fields involved are collinear with respect to one another and the polarization states can be factored out.

When everything is taken into account, after some similar steps shown in Sec. IV, we arrive at the following form for the coincidence counting formula:

$$C_c = A_2 (\gamma P_p L)^2 \frac{\sigma_0^2}{\sigma_p \sqrt{\sigma_p^2 + \sigma_0^2}} I_{\text{cc}}, \tag{36}$$

$$A_2 = \frac{\alpha^2 \pi n^2 A_{\text{eff}}^4}{144 V_Q^{8/3}}, \tag{37}$$

$$I_{\text{cc}} = \frac{1}{L^2} \int_{-L}^{0} dz_1 \int_{-L}^{0} dz_2 \frac{\exp\left[-2i\gamma P_p (z_1 - z_2) - \frac{c' b'^2}{1 + b'^2} + \frac{i}{2} \arctan(b') + \frac{i r'}{1 + b'^2} \right]}{\sqrt{(1 - ik'' \sigma_p^2 z_1)(1 + ik'' \sigma_p^2 z_2)} \sqrt[4]{1 + b'^2}}, \tag{38}$$

where $b' = -k''(z_1 - z_2)\sigma_0^2/2$, $c' = \Delta^2/2\sigma_0^2$, and $r' = -k''(z_1 - z_2)\Delta^2/4$.

From Eqs. (28) and (36), we can see that the single counts and the coincidence counts both scale quadratically with the pump peak power. This is a distinct feature of the $\chi^{(3)}$ interaction, in contrast to the linear dependence on pump power in $\chi^{(2)}$ SPDC. Whereas one might expect to see an exact linear relation between the single counts and the coincidence counts under ideal detection conditions (unity quantum efficiency of the detectors, no loss, no dark counts), the linearity is absent due to the broadband nature of the pump field and the presence of the filters. Some of the correlated twin photons are lost during the filtering process, and some uncorrelated photons are detected instead. The explicit dependence of C_c on the quantity $\sigma_0^2/\sigma_p\sqrt{\sigma_p^2 + \sigma_0^2}$ can be understood from its limiting cases. When the pump bandwidth is wide compared with the filter bandwidth, i.e., $\sigma_p \gg \sigma_0$, every individual frequency component of the pump spectrum will generate its own energy-conserving signal/idler pairs. The filters, being narrow, are only effective at collecting a small portion of the correlated photons. Therefore, the coincidence counts should be proportional to σ_0^2/σ_p^2. On the other hand, if the pump bandwidth is sufficiently narrow, i.e., $\sigma_p \ll \sigma_0$, the photons being filtered (and subsequently collected by the detectors) are more likely to be correlated with each other, in which case the coincidence counts should scale with σ_0/σ_p. Both cases are verified when we look at the asymptotic limits:

$$\lim_{\sigma_p \gg \sigma_0} \frac{\sigma_0^2}{\sigma_p \sqrt{\sigma_p^2 + \sigma_0^2}} = \frac{\sigma_0^2}{\sigma_p^2}, \tag{39}$$

$$\lim_{\sigma_p \ll \sigma_0} \frac{\sigma_0^2}{\sigma_p \sqrt{\sigma_p^2 + \sigma_0^2}} = \frac{\sigma_0}{\sigma_p}. \tag{40}$$

VI. EXPERIMENT VS THEORY

In order to pin down the unknown parameters α and V_Q in Eqs. (29) and (37), we fit our theory to 2 sets of experimental data, where the ratio of pump bandwidth to filter bandwidth is varied. The commonly used least-square fitting technique has been employed. The results are shown in Fig. 4, where the central solid curve corresponds to the optimum fitting parameters, which are determined to be $\alpha = 0.237$ and $V_Q = 1.6 \times 10^{-16}$ m^3. k'' has also been found to be -0.116 ps^2/km, corresponding to the wavelength difference

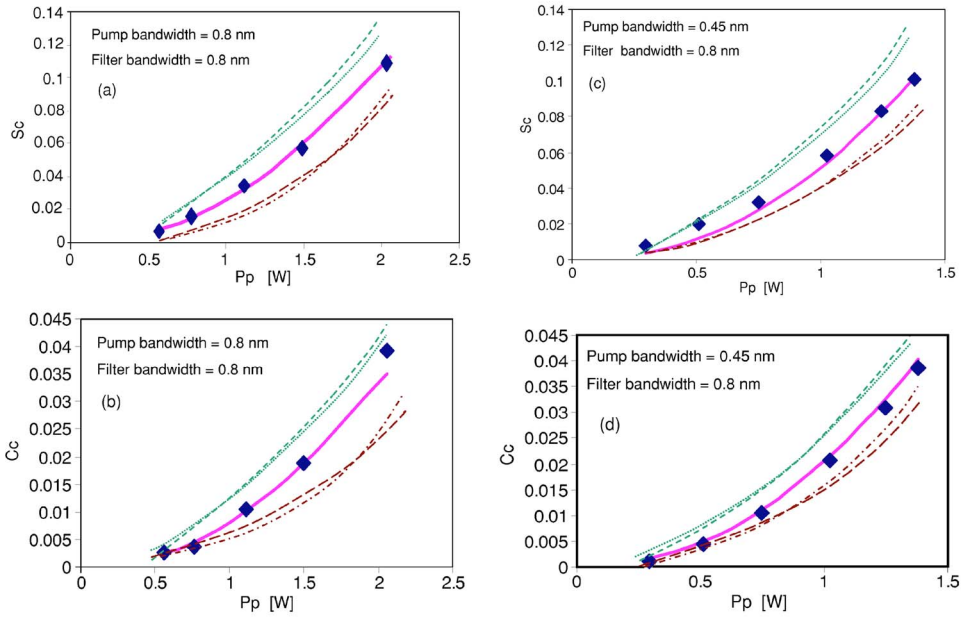

FIG. 4. (Color online) Experiment vs. theory: squares correspond to experimental data and the curves correspond to theoretical predictions. (a): single counts with $\sigma_p=0.8$ nm and $\sigma_0=0.8$ nm; (b): coincidence counts with $\sigma_p=0.8$ nm and $\sigma_0=0.8$ nm; (c): single counts with $\sigma_p=0.45$ nm and $\sigma_0=0.8$ nm; (d): coincidence counts with $\sigma_p=0.45$ nm and $\sigma_0=0.8$ nm. The central solid curve represents the theoretical fit with the optimum fitting parameters ($\alpha=0.237$, $V_Q=1.6\times10^{-16}$ m^3), whereas the other curves correspond to fits with nonoptimum fitting parameters: dotted, $\alpha=0.237$, $V_Q=1.5\times10^{-16}$ m^3; dot-dashed, $\alpha=0.237$, $V_Q=1.7\times10^{-16}$ m^3; short-dashed, $\alpha=0.250$, $V_Q=1.6\times10^{-16}$ m^3; long-dashed, $\alpha=0.220$, $V_Q=1.6\times10^{-16}$ m^3.

$\lambda_p-\lambda_0=1.52$ nm, which agrees well with the measured experimental value. We also show the robustness of the fit by perturbing either one of the fitting parameters around its optimum value by as small as 5%. For example, the dotted curve corresponds to the case where we set $V_Q=1.5\times10^{-16}$ m^3 while keeping α optimum, and the dot-dashed curve corresponds to the case where we set $V_Q=1.7\times10^{-16}$ m^3 while keeping α optimum. The remaining two curves are generated when we keep V_Q optimum and set $\alpha=0.250$ (short-dashed curve), or $\alpha=0.220$ (long-dashed curve), respectively. The large discrepancies between the experiment and the theory induced by this operation are shown in the same figure, which boosts our confidence in the correctness of the theory.

VII. CONCLUSION

We have provided a detailed discussion of the two-photon state originating from the third-order nonlinearity in optical fibers. This $\chi^{(3)}$ two-photon state shares some similar features with the $\chi^{(2)}$ two-photon state generated from SPDC, yet it also has some distinct characteristics. Coincidence photon-counting rate, which is a significant nonclassical figure of merit of the two-photon state, has been shown to depend heavily upon various experimental parameters. The dependence on the ratio of the pump bandwidth to filter bandwidth is of practical importance, because it serves as a guideline for optimizing the measurement of coincidence counts. Single-photon counting rate has also been studied, and both fit to the experimental data reasonably well. While in this paper we are only concerned with parametric fluorescence from a single pump pulse, the current theory can be readily extended to include multi-photon-state generation from one pulse [16], and multiple two-photon-states generation from adjacent pulses [12] to study polarization entanglement. The effect of spontaneous Raman scattering can also be included in our model by taking into account the noninstantaneous nature of the third-order nonlinearity in optical fiber.

ACKNOWLEDGMENTS

The authors would like to thank Dr. Vladimir Grigoryan for valuable discussions. This work is supported in part by the FY2000 Multidisciplinary University Research Initiative through the U.S. Army Research Office, Grant No. DAAD19-00-1-0177.

[1] Y. R. Shen, IEEE J. Quantum Electron. **QE-22**, 1196 (1986).
[2] Govind P. Agrawal, *Nonlinear Fiber Optics*, 3rd ed. (Academic Press, New York, 2001).
[3] Dirk Bouwmeester, Artur Ekert, and Anton Zeilinger, *The Physics of Quantum Information: Quantum Cryptography, Quantum Teleportation, Quantum Computation*, 1st ed. (Springer-Verlag, Berlin, 2000).
[4] Paul L. Voss and Prem Kumar, Opt. Lett. **29**, 445 (2004).
[5] Xiaoying Li, Jun Chen, Paul L. Voss, Jay E. Sharping, and Prem Kumar, Opt. Express **12**, 3737 (2004).
[6] Morton H. Rubin, David N. Klyshko, Y. H. Shih, and A. V. Sergienko, Phys. Rev. A **50**, 5122 (1994).
[7] Timothy E. Keller and Morton H. Rubin, Phys. Rev. A **56**, 1534 (1997).
[8] A. K. Ekert, Phys. Rev. Lett. **67**, 661 (1991).
[9] C. H. Bennett, G. Brassard, C. Crèpeau, R. Jozsa, A. Peres, and W. K. Wootters, Phys. Rev. Lett. **70**, 1895 (1993).
[10] R. J. Glauber, Phys. Rev. **130**, 2529 (1963); **131**, 2766 (1963).
[11] M. Fiorentino, P. L. Voss, J. E. Sharping, and P. Kumar, IEEE Photonics Technol. Lett. **14**, 983 (2002).
[12] Xiaoying Li, Paul L. Voss, Jay E. Sharping, and Prem Kumar, Phys. Rev. Lett. **94**, 053601 (2005).
[13] David B. Mortimore, J. Lightwave Technol. **6**, 1217 (1988).
[14] Jeffrey H. Shapiro, IEEE J. Quantum Electron. **QE-21**, 237 (1985).
[15] I. S. Gradshteyn and I. M. Ryzhik, *Table of Integrals, Series, and Products*, 6th ed. (Academic Press, San Diego, 2000) where the formula of interest is (3.923).
[16] Manfred Eibl, Sascha Gaertner, Mohamed Bourennane, Christian Kurtsiefer, Marek Zukowski, and Harald Weinfurter, Phys. Rev. Lett. **90**, 200403 (2003).